Inorganic Chemistry
Article

Inorg. Chem. **2010**, *49*, 4149–4155 **4149**
DOI: 10.1021/ic902201u

Vertex and Edge Truncated Octahedron Gold Crystals. *N*-alkylimidazole and Silver(I) Ion Controlled Morphology Transformation

S. J. Hsu, Padi Y. S. Su, L. Y. Jian, A. H. H. Chang, and Ivan J. B. Lin*

Department of Chemistry and Nanotechnology Research Center, National Dong Hwa University, Shoufeng, Hualien 974, Taiwan

Received November 6, 2009

Two interesting morphology transformations of Au crystals are observed through reacting a mixture of *N*-alkylimidazole (denoted as C_n-im, where $C_n = C_nH_{2n+1}$, and $n = 18$ and 1), $AgNO_3$, and $HAuCl_4$ at 200 °C. The long chain C_{18}-im with increasing $AgNO_3$ concentration leads to a progressive truncation of octahedrons at {100} vertices to produce cubes. On the other hand, increasing the concentrations of C_1-im and $AgNO_3$, results in a progressive truncation of octahedrons at {110} edges to give rhombic dodecahedrons, which further transform to the unprecedented tetrahexahedrons. The phenomenon could be understood by considering that while both C_{18}-im and C_1-im function as a capping agent with preferential adsorption on Au {111} facets, Ag^+ adsorbs and is subsequently reduced to Ag on Au {110} facets for the sterically demanding C_{18}-im, but on the Au {100} facets for C_1-im. The competition between the growth of the facets protected by imidazole and Ag controls the morphology transformation via truncation of octahedrons at vertices or edges.

Introduction

For a face-centered cubic lattice, the relative surface energies (γ) generally follow the order $\gamma_{110} > \gamma_{100} > \gamma_{111}$, proportional to the surface atom density. The high energy surface is more reactive, such that crystals with {111} facets are thermodynamically preferred.[1] Addition of capping agents may influence the surface energies of the adsorbed facets and subsequently the growth of crystals,[2] therefore a proper choice of capping agents could control the Au crystal morphology.[3−6] Preferential adsorption of capping agents to a specific crystal plane would stabilize the surface energy of that plane, on which further deposition by Au is suppressed. As a result, the perpendicular growth on the stabilized crystal plane is inhibited, and the parallel growth is enhanced, which increases the surface area of the protected plane. Many capping agents are known, including surfactants,[3] polymers,[4] biomolecules,[5] and long chain donor ligands.[6]

Recently trace amount of Ag^+ ions has been used to control the morphology of Au nanocrystals (NCs).[7,8] Cases in which Ag^+ assists the growth of Au nanorods in seed-mediated aqueous surfactant solutions were reported.[8] It has been suggested that in the presence of cetyl-trimethyl-ammonium bromide (CTAB), selective deposition of Ag on

*To whom correspondence should be addressed. E-mail: ijblin@mail.ndhu.edu.tw. Phone: +886-3-863-3599. Fax: +886-3-863-3570.

(1) (a) Wang, Z. L. *J. Phys. Chem. B* **2000**, *104*, 1153. (b) Wiley, B.; Sun, Y.; Mayers, B.; Xia, Y. *Chem.—Eur. J.* **2005**, *11*, 454.
(2) (a) Yu, S. H. *Top. Curr. Chem.* **2007**, *271*, 79. (b) Yu, S. H.; Cölfen, H. *J. Mater. Chem.* **2004**, *14*, 2124.
(3) (a) Esumi, K.; Hara, J.; Aihara, N.; Usui, K.; Torigoe, K. *J. Colloid Interface Sci.* **1998**, *208*, 578. (b) Gao, J.; Bender, C. M.; Murphy, C. J. *Langmuir* **2003**, *19*, 9065. (c) Zhang, L.; Sun, X.; Song, Y.; Jiang, X.; Dang, S.; Wang, E. *Langmuir* **2006**, *22*, 2838. (d) Bakshi, M. S.; Possmayer, F.; Petersen, N. O. *Chem. Mater.* **2007**, *19*, 1257. (e) Bakshi, M. S.; Kaur, G.; Thakur, P.; Banipal, T. S.; Possmayer, F.; Petersen, N. O. *J. Phys. Chem. C* **2007**, *111*, 5932. (f) Zhao, N.; Wei, Y.; Sun, N.; Chen, Q.; Bai, J.; Zhou, L.; Qin, Y.; Li, M.; Qi, L. *Langmuir* **2008**, *24*, 991.
(4) (a) Xiong, Y.; Washio, I.; Chen, J.; Cai, H.; Li, Z. Y.; Xia, Y. *Langmuir* **2006**, *22*, 8563. (b) Zheng, P.; Jiang, X.; Zhang, X.; Zhang, W.; Shi, L. *Langmuir* **2006**, *22*, 9393. (c) Umar, A. A.; Oyama, M. *Cryst. Growth Des.* **2006**, *6*, 818. (d) Abraham, S.; Kim, I.; Batt, C. A. *Angew. Chem., Int. Ed.* **2007**, *46*, 5720. (e) Hansen, C. R.; Westerlund, F.; Moth-Poulsen, K.; Ravindranath, R.; Valiyaveettil, S.; Bjornholm, T. *Langmuir* **2008**, *24*, 3905. (f) Tang, X. L.; Jiang, P.; Ge, G. L.; Tsuji, M.; Xie, S. S.; Guo, Y. J. *Langmuir* **2008**, *24*, 1763.
(5) (a) Yang, T.; Li, Z.; Wang, L.; Guo, C.; Sun, Y. *Langmuir* **2007**, *23*, 10533. (b) Xie, J.; Lee, J. Y.; Wang, D. I. C. *J. Phys. Chem. C* **2007**, *111*, 10226. (c) Chen, Y. M.; Yu, C. J.; Cheng, T. L.; Tseng, W. L. *Langmuir* **2008**, *24*, 3654.
(6) (a) Huo, Z.; Tsung, C. K.; Huang, W.; Zhang, X.; Yang, P. *Nano Lett.* **2008**, *8*, 2041. (b) Lu, X.; Yavuz, M. S.; Tuan, H. Y.; Korgel, B. A.; Xia, Y. *J. Am. Chem. Soc.* **2008**, *130*, 8900–8901.
(7) (a) Xiang, Y.; Wu, X.; Liu, D.; Feng, L.; Zhang, K.; Chu, W.; Zhou, W.; Xie, S. *J. Phys. Chem. C* **2008**, *112*, 3203. (b) Smith, D. K.; Korgel, B. A. *Langmuir* **2008**, *24*, 644. (c) Seo, D.; Park, J. C.; Song, H. *J. Am. Chem. Soc.* **2006**, *128*, 14863. (d) Seo, D.; Yoo, C. I.; Park, J. C.; Park, S. M.; Ryu, S.; Song, H. *Angew. Chem., Int. Ed.* **2008**, *47*, 763. (e) Seo, D.; Park, J. H.; Jung, J.; Park, S. M.; Ryu, S.; Kwak, J.; Song, H. *J. Phys. Chem. C* **2009**, *113*, 3449.
(8) (a) Jana, N. R.; Gearheart, L.; Murphy, C. J. *Adv. Mater.* **2001**, *13*, 1389. (b) Nikoobakht, B.; El-Sayed, M. A. *Chem. Mater.* **2003**, *15*, 1957. (c) Liu, M. Z.; Guyot-Sionnest, P. *J. Phys. Chem. B* **2005**, *109*, 22192. (d) Song, J. H.; Kim, D.; Yang, P. *Chem.—Eur. J.* **2005**, *11*, 910. (e) Orendorff, C. J.; Murphy, C. J. *J. Phys. Chem. B.* **2006**, *110*, 3990. (f) Kou, X.; Zhang, S.; Tsung, C. K.; Yang, Z.; Yeung, M. H.; Stucky, G. D.; Sun, L.; Wang, J. F.; Yan, C. *Chem.—Eur. J.* **2007**, *13*, 2929. (g) Keul, H. A.; Moller, M.; Bockstaller, M. R. *Langmuir* **2007**, *23*, 10307. (h) Chen, H. M.; Liu, R.-S.; Tsai, D. P. *Cryst. Growth Des.* **2009**, *9*, 2079. (i) Jiang, X. C.; Pileni, M. P. *Colloid Surf., A* **2007**, *295*, 228.

Published on Web 04/05/2010

the {110} facets of Au single crystalline seeds slowed down the growth along the norm of the {110} side facets of the rods, but elevated the growth on the facets at two ends, and consequently favored the formation of single crystalline nanorods. Similar Ag^+ assisted Au nanorod formation by electrochemical[9] and photochemical[10] methods have also been investigated. The effect of Ag^+ in the fabrication of gold crystals has been attributed to a phenomenon known as Ag underpotential deposition (UPD).[11] That is, the reduction of Ag^+ to Ag at a metal substrate of specific surface has a potential less than the standard reduction potential of Ag^+. Different capping agents might alter the preferential Ag deposition on Au crystal surfaces. For instance, in the presence of poly(vinyl pyrrolidone) (PVP), preferential Ag deposition on Au {100} rather than on {110} facets was proposed to suppress the growth along the norm of the {100} facets.[7c−e] With a combination of PVP and $AgNO_3$, the morphology of Au polyhedrons between octahedron and cube was controlled,[7c,d] and multitwinned Au nanorods with five {100} side facets were formed.[7e]

Imidazole derivatives, commonly found in biological systems, have been broadly employed in the medicinal chemistry.[12] Easily accessed *N*-alkyl imidazoles are also versatile ligands toward coinage metal ions.[13,14] Recent advancement shows that whereas *N*-methyl imidazoles could stabilize Au nanoparticles (NPs) in ionic liquid,[15] long chain *N*-alkyl imidazoles could be utilized to form gold containing liquid crystals, to stabilize AuNPs in solution, and to fabricate Au nanoplatelets through thermolysis.[14]

In this work, by varying $AgNO_3$ concentrations and *N*-alkyl chain length of imidazole in the thermolysis with $HAuCl_4$, octahedron-symmetric Au crystals with truncation at vertices or edges are tuned. When *N*-octadecyl imidazole (denoted as C_{18}-im) is employed, increasing the $AgNO_3$ concentration leads to a progressive truncation of octahedrons at vertices to form cubes. On the other hand, as *N*-methylimidazole (denoted as C_1-im) is utilized, raising the $AgNO_3$ concentration causes a progressive truncation at the edges of octahedrons to produce rhombic dodecahedrons, which further transform to tetrahexahedrons (THHs). Very recently synthesis of nanosized Au rhombic dodecahedrons has appeared;[16,17] however, the progression through truncation of octahedrons at edges covered with {110} of high surface energy as seen in the present work, has not been observed. Furthermore the synthesis of fine THH gold covered with high-index {210} planes is unprecedented.

Experimental Section

Chemicals. Compounds C_1-im, $AgNO_3$, and $HAuCl_4$ were purchased from Aldrich. Compound C_{18}-im was prepared by the known methods.[18]

Typical Method for the Preparation of Thermolysis Precursor. C_{18}-im (0.38 g, 1.2 mmol) and $HAuCl_4$ (0.10 g, 0.3 mmol) were dissolved in EtOH (50 mL), and were mixed with $AgNO_3$ (1.70 mg, 0.01 mmol) in 10 mL of EtOH. After stirring the resultant solution for 1 h, EtOH was removed by rotary evaporator and the residue was dried under vacuum for 2 h. This mixture contains C_{18}-im, $HAuCl_4$, and $AgNO_3$ with molar ratios of 120/30/1. To fabricate Au crystals, the resultant mixture was heated at 200 °C for 1 h in a sealed glass tube or sample vial. The residue was washed several times with EtOH and DMSO and collected. Samples with $HAuCl_4$ up to 1.0 g worked equally well.

Equipment and Analysis. Transmission electron microscopy (TEM) and corresponding electron diffraction (ED) and energy-dispersive X-ray spectroscopy (EDX) patterns were obtained on a JEOL JEM-3010 TEM operated at 300 KV. Scanning electron microscopy (SEM) images were obtained using a JEOL JEM-6500F operated at 15 KV. X-ray diffraction (XRD) patterns were measured on a D8 Advanced Bruker and XRD Rigaku D/max-2500 diffractometer using Cu K_α radiation. MALDI mass analysis was performed on a Bruker Daltonics Autoflex MALDI-TOF system.

Theoretical Method. The calculation of density function B3LYP[19a,b] with LanL2DZ[19c] basis sets are carried out to obtain the binding energies of Ag^+Au_5, Ag^+Au_4, and Ag^+Au_3. With basis set LanL2DZ, the ab initio effective core potentials are employed to replace the core electrons of Au and Ag, in which mass-velocity and Darwin relativisitic effects have been incorporated. The Gaussian 03 program[20] was utilized in the ab initio electronic structure calculations.

Results

At room temperature the mixture of C_{18}−Im, $HAuCl_4$, and $AgNO_3$ is a yellowish powder, while that with C_1-im a viscous paste. Upon heating to 200 °C, they all become clear yellow liquid. As thermolysis proceeds, the color turns to brown and the viscosity increases. For the C_{18}-im mixture, shining gold particles appear at about 12 min, and those for the C_1-im mixture around 2 min. At the end of the reaction (1 h) at room temperature, they form a fused solid with micrometer and submicrometer sized metallic gold at the bottom. Interestingly, no AgCl precipitate is observed under the reaction conditions, suggesting that AgCl is soluble in this system. In general, thermolysis is a process that molecular precursors undergo thermal decomposition without solvent. Examples of fabricating AuNPs through thermolysis of Au(I)/(III) complexes have been reported.[14,21] Compared to the numerous solution processes of fabricating AuNPs,[22] high temperature, high viscosity, and high metal content are typical for a thermolysis process. Although $HAuCl_4$ itself

(9) Mohamed, M. B.; Ismail, K. Z.; Link, S.; El-Sayed, M. A. *J. Phys. Chem. B* **1998**, *102*, 9370.
(10) Kim, F.; Song, J. H.; Yang, P. *J. Am. Chem. Soc.* **2002**, *124*, 14316.
(11) Herrero, E.; Buller, L. J.; Abrun, H. D. *Chem. Rev.* **2001**, *101*, 1897.
(12) Rezaei, Z.; Khabnadideh, S.; Pakshir, K.; Hossaini, Z.; Amiri, F.; Assadpour, E. *Eur. J. Med. Chem.* **2009**, *44*, 3064.
(13) (a) Mirica, L. M.; Ottenwaelder, X.; Stack, T. D. P. *Chem. Rev.* **2004**, *104*, 1013. (b) Huang, X. C.; Zhang, J. P.; Chen, X. M. *Cryst. Growth Des.* **2006**, *6*, 1194. (c) Lee, C. K.; Ling, M. J.; Lin, I. J. B. *Dalton Trans.* **2003**, 4731. (d) Lee, C. K.; Hsu, K. M.; Tsai, C. H.; Lai, C. K.; Lin, I. J. B. *Dalton Trans.* **2004**, 1120.
(14) Hsu, S. J.; Hsu, K. M.; Leong, M. K.; Lin, I. J. B. *Dalton Trans.* **2008**, 1924.
(15) Dash, P.; Scott, R. W. J. *Chem. Commun.* **2009**, 812.
(16) Zheng, W.; Niu, S.; Wang, D.; Liu, X.; Li, H.; Han, S.; Chen, J.; Tang, Z.; Xu, G. *J. Am. Chem. Soc.* **2009**, *131*, 697.
(17) Kim, D. Y.; Im, S. H.; Park, O. O.; Lim, Y. T. *CrystEngComm* **2010**, *12*, 116.
(18) Khabnadideh, S.; Rezaei, Z.; Khalafi-Nezhad, A.; Bahrinajafi, R.; Mohamadi, R.; Farrokhroz, A. A. *Bioorg. Med. Chem. Lett.* **2003**, *13*, 2863.
(19) (a) Becke, A. D. *J. Chem. Phys.* **1993**, *98*, 5648. (b) Lee, C.; Yang, W.; Parr, R. G. *Phys. Rev. B* **1998**, *37*, 785. (c) Hay, P. J.; Wadt, W. R. *J. Chem. Phys.* **1985**, *82*, 299.
(20) Frisch, M. J. et al. *GAUSSIAN 03*, Revision C.02; Gaussian, Inc.: Wallingford, CT, 2004.
(21) (a) Yamamoto, M.; Nakamoto, M. *Chem. Lett.* **2003**, *32*, 452. (b) Nakamoto, M.; Kashiwagi, Y.; Yamamoto, M. *Inorg. Chim. Acta* **2005**, *358*, 4229. (c) Gomez, S.; Philippot, K.; Collière, V.; Chaudret, B.; Senocq, F.; Lecante, P. *Chem. Commun.* **2000**, *19*, 1945. (d) Nakamoto, M.; Yamamoto, M.; Fukusumi, M. *Chem. Commun.* **2002**, *15*, 1622.
(22) Daniel, M. C.; Astruc, D. *Chem. Rev.* **2004**, *104*, 293.

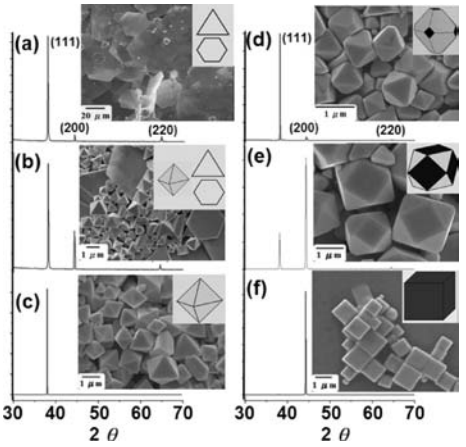

Figure 1. SEM images and XRD spectra of gold crystals obtained with a fixed [C_{18}-im]/[Au] = 4/1 and at [Ag]/[Au] ratios of (a) 1/600, (b) 1/50, (c) 1/45, (d) 1/40, (e) 1/35, and (f) 1/30. Schematic drawing of major morphologies observed in each SEM image is given as an inset.

could undergo thermal decomposition to produce Au clumps, in this work, the addition of imidazole and $AgNO_3$ provides a simple alternative route for the reduction of Au(III) to Au metal with shapes, in which imidazole functions as a solvent, a ligand, a reductant, and a capping agent. Here, Au(III)-imidazole complexes formed in situ undergo decomposition reaction in the coordinating solvent of imidazole at high temperature. MALDI-TOF spectrum (Supporting Information, Figure S1) for the organic products shows among others an m/z peak of 640.0, corresponding to a monoprotonated cation of imidazole dimer, possibly formed via oxidative C−C coupling of imidazole at the C^2-position followed by protonation (eq 1). In addition to the protonated C_{18}-im at m/z of 321.7, other major products show m/z peaks at 574.0 and 387.8. The former is assumed to be a dialkyl imidazolium cation, and the latter a protonated cation of imidazole dimer with only one $C_{18}H_{37}$ chain. Previously, thermolysis of thiolato Au complexes to fabricate AuNPs has been reported, in which disulfides were formed via oxidative coupling of the thiolate ligands.[21b]

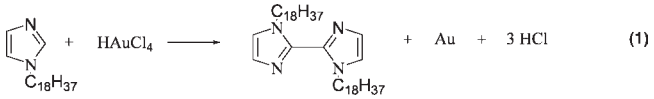

(1)

Thermolysis of different ratios of [C_{18}-im]:[$HAuCl_4$]:[$AgNO_3$] (denoted as [C_{18}-im]/[Au]/[Ag]) produces various crystalline Au morphologies. SEM images and diffractograms for the products carried out at [C_{18}-im]/[Au] = 4/1 with incremental additions of $AgNO_3$ are shown in Figure 1. Schematic drawing illustrating the major morphologies observed in each image is given as an inset. At low $AgNO_3$ concentration, that is, with an [Ag]/[Au] ratio of 1/600, the major morphology is micrometer-sized triangular and hexagonal platelets (Figure 1a). The diffractogram of the products shows a strong (111) and weak (200) and (220) reflections (Figure 1a). At the [Ag]/[Au] ratio of 1/50, micrometer and submicrometer sized octahedrons (major), platelets (minor), and other faceted particles (traces) are observed (Figure 1b). The corresponding diffractogram exhibits a strong (111), a medium (200), and a very weak (220) peak (Figure 1b). Changing the [Ag]/[Au] ratio to 1/45, octahedron morphology becomes overwhelming, and the

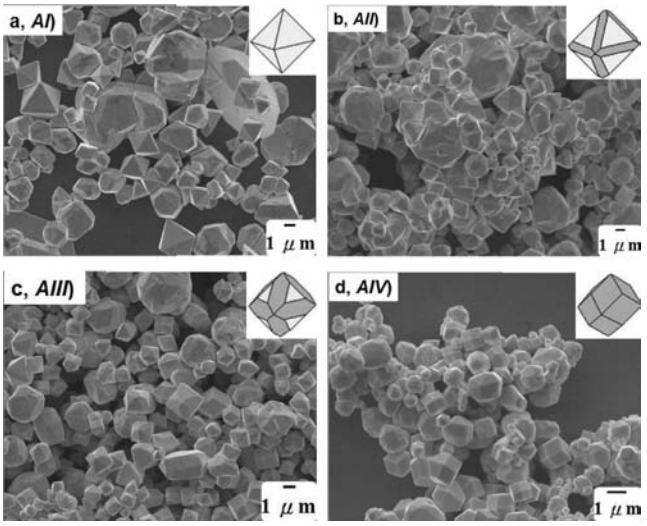

Figure 2. SEM images of gold crystals obtained with a fixed [C_1-im]/[Au] = 4/1 and at [Ag]/[Au] ratios of (a) 1/600, (b) 1/50, (c) 1/40, and (d) 1/30. Insets show schematic drawings of octahedron, edge-truncated octahedron (octahedral dominant), edge-truncated octahedron (dodecahedron dominant), and rhombic dodecahedron observed in (a), (b), (c), and (d), respectively.

diffractogram shows a strong (111) and a very weak (200) reflection (Figure 1c). With a further increment of $AgNO_3$ ([Ag]/[Au] = 1/40), vertex-truncated octahedrons are produced, of which the truncated vertices are covered with {100} facets (Figure 1d). A strong (111) and a weak (200) reflection observed in the diffractogram are consistent with the results of SEM (Figure 1d). When the ratio of [Ag]/[Au] is 1/35, cuboctahedrons are formed; the diffractogram shows a strong (200) peak along with a medium (111) peak (Figure 1e). For a perfect cuboctahedron, the area ratio of {100}:{111} is 1:0.58; the observation of a weaker than anticipated (111) intensity may indicate that mostly the {100} surfaces of the cuboctahedrons are lying parallel to the substrate. Full development of gold cubes covered with six {100} facets is achieved when the [Ag]/[Au] ratio is 1/30; the corresponding diffractogram shows predominantly the (200) peak (Figure 1f). When the [Ag]/[Au] ratio is 1/1, particles are sphere-like. It appears that at a [C_{18}-im]/[Au] ratio of 4/1, increasing the $AgNO_3$ concentration from the [Ag]/[Au] ratio of 1/600 up to 1/30 changes the morphology of Au crystals progressively from platelet to octahedron, to vertex-truncated octahedron, to cuboctahedron, then eventually to cube. Although morphological conversion from octahedron to cube is known in the Ag^+ assisted polyol process,[7c,d] the present work is the first example of utilizing C_{18}-im and $AgNO_3$ to provide a wider range of morphology from platelet to cube through thermolysis.

Interestingly, while C_{18}-im and $AgNO_3$ regulate the growth of O_h symmetric Au {111} and {100} surfaces as described in the previous paragraph, C_1-im and $AgNO_3$ regulate the growth of {111} and {110} surfaces. Different ratios of [C_1-im]/[Au] and [Ag]/[Au] have been studied. To better elucidate these ratio-combinations, labels ***A***, ***B*** and ***C*** are used to stand for the [C_1-im]/[Au] ratios of 4/1, 8/1, and 12/1, respectively, and ***I***, ***II***, ***III*** and ***IV*** are used to represent [Ag]/[Au] ratios of 1/600, 1/50, 1/40, and 1/30, respectively. SEM images for the products from series ***AI-AIV*** are shown in Figure 2. Selected areas showing O_h symmetric crystals are

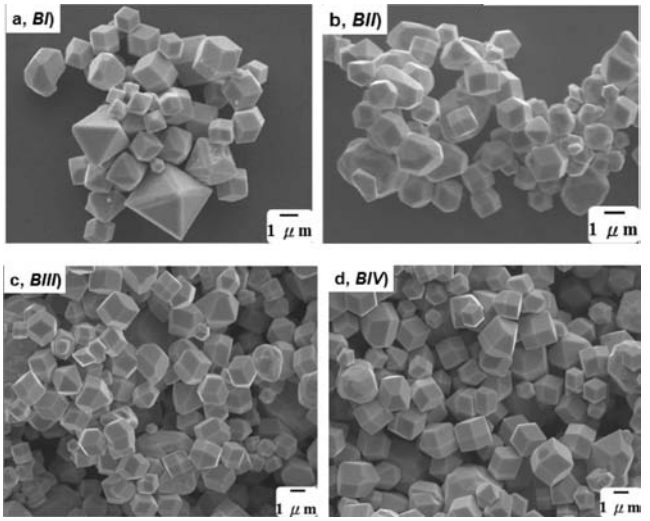

Figure 3. SEM images of gold crystals obtained with a fixed [C_1-im]/[Au] = 8/1 and at [Ag]/[Au] ratios of (a) 1/600, (b) 1/50, (c) 1/40, and (d) 1/30.

given in insets. The major product of ***AI*** is irregularly faceted particles (ca. 75%), and the minor product is micrometer- and submicrometer-sized perfect octahedrons with sharp edges and corners (ca. 25%) (Figure 2a). In entry ***AII***, other than irregular faceted particles (ca. 70%), the incremental addition of $AgNO_3$ leads to the formation of unusual edge-truncated octahedrons (octahedron dominant, ca. 30%), whose truncated edges are covered with {110} facets (Figure 2b). This is the first report that such Au crystals are prepared in the laboratory; it is noted that octahedronal Au crystals with truncation at edges are only known in natural minerals.[23] In ***AIII***, further increasing the $AgNO_3$ concentration results in an increase in the surface area of edge-truncation at octahedron and thus generates a dodecahedron dominant morphology (ca. 35%), in which the area of {110} facets is more than that of the {111} (Figure 2c). Subsequently in ***AIV***, complete edge-truncation of octahedron leads to the formation of about 40% of rhombic dodecahedrons, which are covered with twelve {110} facets (Figures 2d). The composition of gold in these rhombic dodecahedrons is confirmed by EDX, which shows characteristic peaks assigned to gold.

Series ***B*** has twice the C_1-im concentration over that of ***A***. SEM images for the products indicate that lesser $AgNO_3$ is required for ***B*** to increase the {110} surfaces at the truncated edge as compared to ***A*** (Figure 3). Thus while O_h symmetric morphologies of edge-truncated octahedrons and rhombic dodecahedrons are observed in ***BI***, only rhombic dodecahedrons are found in ***BII***, ***BIII***, and ***BIV***. We also notice that increasing the $AgNO_3$ concentration from ***BI*** to ***BIV*** increases the population of rhombic dodecahedrons. As estimated from SEM images, about 30% of rhombic dodecahedrons are found in ***BI***, and about 40%, 50%, and 60% populations of rhombic dodecahedrons are observed in ***BII***, ***BIII***, and ***BIV***, respectively.

Series ***C*** has tripled the C_1-im concentration over that of ***A***. As indicated in Figure 4, the proportion of rhombic dodecahedrons increases gradually from ***CI*** to ***CII***, ***CIII***, and ***CIV*** with values of about 35%, 50%, 60%, and 70%, respectively, as the $AgNO_3$ concentration increases. Further increasing the $AgNO_3$ concentration to 1/20 molar ratio with respect to $HAuCl_4$, gives rhombic dodecahedrons in highest yield (ca. 80%) (Figure 4e). When the $AgNO_3$ concentration is 1/15 ratio, for the first time Au crystals with {210} high-index planes of THH (ca. 25%) are synthesized (Figure 4f), despite that natural occurring Au THH is known.[23] It is not until recently that Pt THH NCs have been synthesized.[24] The unsaturated high-index crystal surfaces possess enhanced catalytic activity than common, stable, and low-index planes such as {111} and {100}.

Diffractograms of the ***A***, ***B***, and ***C*** series are given in Figure 5. It is noted that (1) increasing the $AgNO_3$ concentration (from ***I*** to ***IV***) increases the intensity of (220) reflections gradually in all ***A***, ***B***, and ***C*** series, (2) the increase in the (220) reflection is more substantial going from ***A*** to ***B*** and ***C***, and (3) although {111} is the most stable surface in fcc system, (220) reflection is however the dominant peak in ***BIII***, ***BIV***, ***CIII***, and ***CIV***. All these observations are consistent with the results observed from SEM that increasing the $AgNO_3$ and C_1-im concentrations enhances the formation of {110} surface areas.

Discussion

The results described in the previous section indicate that changing the chain length from C_{18}-im to C_1-im drastically alters the morphology transformation pathway. Scheme 1 summarizes the conversion of Au crystals with incremental addition of $AgNO_3$ to the [C_{18}-im]/[Au] = 4/1 mixture, in which both C_{18}-im and Ag^+ play a key role. Previously we reported a simple method to produce large Au platelets with {111} facets through thermolysis of a mixture of C_{18}-im and $HAuCl_4$ without $AgNO_3$.[25] It has been proposed that the capping agent C_{18}-im, which adsorbed preferentially on Au {111} facets, also functioned as a lamellar template through hydrophobic chain−chain interactions, and therefore favored the formation of extended platelets. In the present work, at the [Ag]/[Au] ratio of 1/600, the concentration of $AgNO_3$ is too low to have significant influence on the role of C_{18}-im in the growth of Au crystals. Consequently, image of platelets and diffractogram of strong (111) reflection are seen in Figure 1a. $AgNO_3$ affects the role of C_{18}-im at the [Ag]/[Au] ratios of 1/50 and 1/45, at which octahedrons rather than platelets become the major products. Apparently, in the presence of Ag^+, C_{18}-im still preferentially protects the Au{111} facets during the growth process, as evidenced by the major (111) reflections in Figure 1b and 1c. However, the templating effect of C_{18}-im is interfered with perhaps because of the competition of Ag^+ adsorption on the Au cluster facets. As the [Ag]/[Au] ratio is raised further up to 1/30, a sequential truncation of octahedron at vertices leads to the formation of octahedrons, cuboctahedrons, and cubes. In this transformation, crystals with {111} dominant progressively turn to {100} dominant. This morphology transformation is similar to that of the Ag^+ ion assisted and seed-mediated polyol process reported by Song and co-workers.[7c,d] In that example, with capping agent PVP, Ag^+ could tune the morphology of Au NCs from octahedron (with 8 {111} facets) to cube (with 6 {100} facets) through vertex truncation. Selective Ag UPD on Au {100} facets in the presence of PVP has been suggested to suppress the growth along the

(23) Taber, S. *Am. Mineral.* **1942**, *27*, 219.

(24) Xiong, Y.; Wiley, B. J.; Xia, Y. *Angew. Chem., Int. Ed.* **2007**, *46*, 7157.

(25) Hsu, S. J.; Lin, I. J. B. *J. Chin. Chem. Soc.* **2009**, *56*, 98.

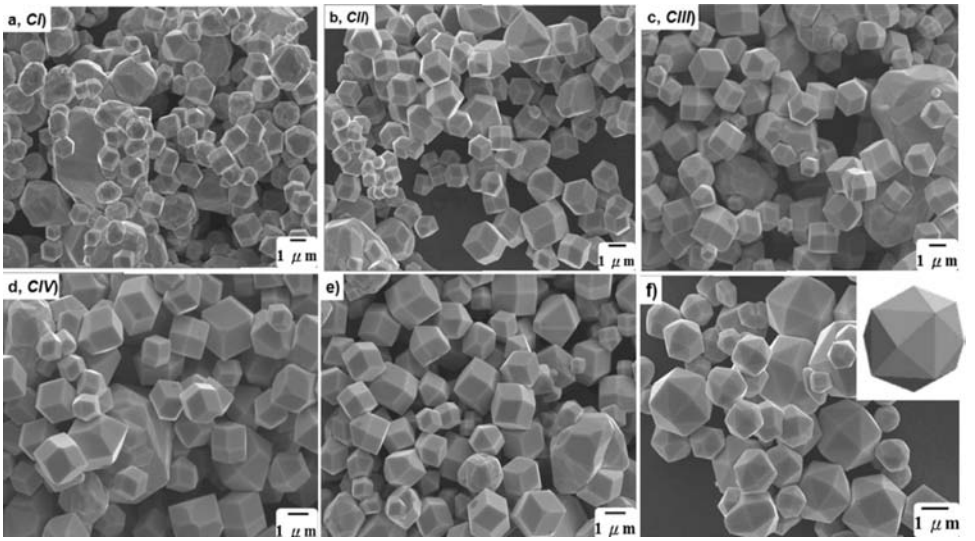

Figure 4. SEM images of gold crystals obtained with a fixed [C_1-im]/[Au] = 12/1 and at [Ag]/[Au] ratios of (a) 1/600, (b) 1/50, (c) 1/40 (d) 1/30, (e) 1/20, and (f) 1/15 with a THH crystal given in the inset.

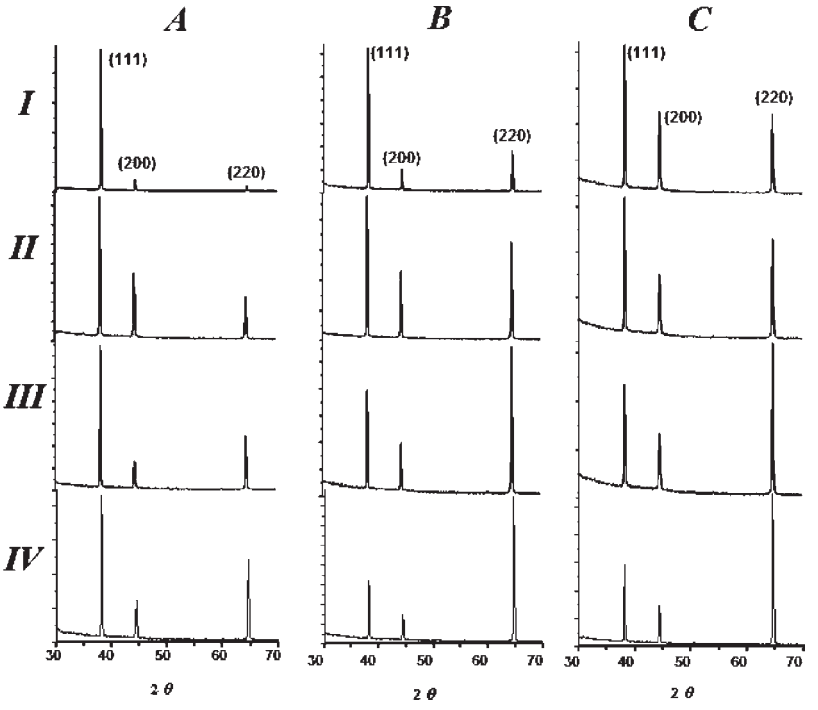

Figure 5. XRD spectra of gold crystals were obtained with different ratios of [C_1-im]/[Au] (A = 4/1, B = 8/1, C = 12/1), and different ratios of [Ag]/[Au] (I = 1/600, II = 1/50, III = 1/40, IV = 1/30).

norm of the {100} facets but increase the area of {100} facets. It followed that the relative growth rate between the {111} and {100} facets regulated the transformation of morphology between octahedron and cube.[26] Although a similar argument could be applied to the present work, two major questions remain to be answered. The first question concerns the nature of interaction between Ag^+ and colloidal Au surfaces. To better understand this issue, a simple estimation of the binding energy between Ag^+ and clean Au surface is made by performing density functional theory calculations. Specifically, the binding pattern between Ag^+ and Au surface of {110}, {100} and {111}, is simulated by the arrangement of Ag^+Au_5, Ag^+Au_4, and Ag^+Au_3, as seen in Figure 6 and Supporting Information, Table S1, whose favorable binding energies are obtained by taking the energy difference with separated $Ag^+ + Au_5$, $Ag^+ + Au_4$, and $Ag^+ + Au_3$, respectively, with B3YLP/LanL2DZ calculations. The result suggests among others a trend of {110} > {100} > {111} for binding energy. The adsorbed Ag^+ could be subsequently reduced to Ag on the Au facets via the known phenomenon of UPD. Calculation reported by Sanchez et al[27] suggested that the shifts of Ag UPD are in the order {110} > {100} > {111},

(26) Habas, A. R.; Tao, S.; Yang, P. *Small* **2008**, *4*, 310.

(27) (a) Sanchez, C. G.; Del Popolo, M. G.; Leiva, E. P. M. *Surf. Sci.* **1999**, *421*, 59. (b) Rojas, M. I.; Sanchez, C. G.; Del Popolo, M. G.; Leiva, E. P. M. *Surf. Sci.* **2000**, *453*, 225.

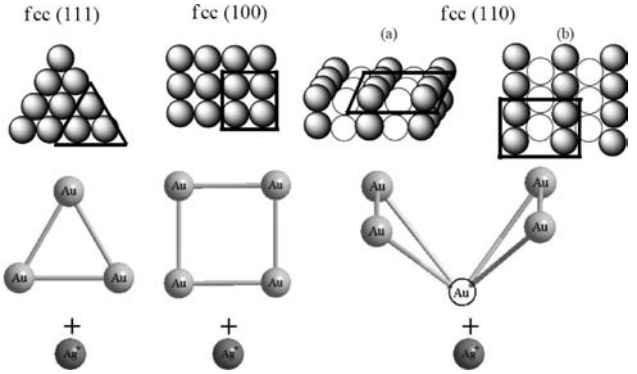

Figure 6. Interaction between Ag^+ and three Au {111}, {100}, {110} facets are shown schematically, where (a) and (b) are the side- and top-views, respectively. The boxed Au clusters are utilized in the estimation of binding energies by density functional theory.

Scheme 1. Change of Au Crystalline Morphologies upon Incremental Addition of $AgNO_3$ to a [C_{18}-im]/[Au] Mixture at Molar Ratio of 4/1

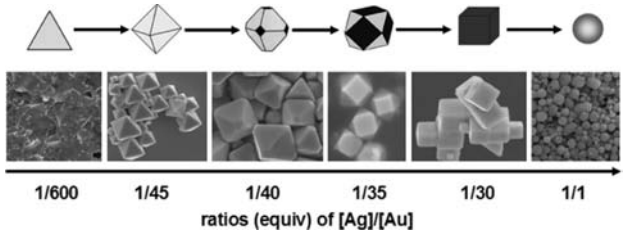

which parallels the order of binding energy between Ag^+ and Au facets. As mentioned in the introduction, experiments to support the Ag UPD on Au {110} facets are numerous. Thus the second question: why in our work, the most favorable UPD shift does not occur on the expected Au {110} facets. We propose that the long alkyl chain of the capping agent C_{18}-im sterically inhibits the Ag^+ ion to adsorb in the ditch of the {110} facets (Figure 6), but in turn prefers the Ag^+ adsorption on the sterically more favorable, though energetically less favorable Au {100}. Underpotential reduction of Ag^+ to Ag then occurs on the Au {100} facets. Although the deposited Ag could undergo galvanic exchange reaction with Au (I)/(III) ions, further deposition of Au on these facets would be slowed down, compared to the conditions without Ag deposition. Therefore C_{18}-im and $AgNO_3$ could promote the growth parallel to the Au {111} and {100} facets, respectively. The different growth rates of these two facets, regulated by the concentrations of C_{18}-im and $AgNO_3$, could explain the formation of different O_h symmetric structures. At the [Ag]/[Au] ratio of 1/1, however, the Ag^+ UPD does not seem to play a role that only spherical particles are produced. Similar results were found previously.[7c]

Scheme 2 summarizes the structural transformation of Au crystals with incremental additions of $AgNO_3$ and C_1-im. Morphology transformation from octahedron to edge-truncated octahedron (octahedron dominant), edge-truncated octahedron (dodecahedron dominant), rhombic dodecahedron, and THH are observed. Diffractograms in Figure 5 show that increasing the C_1-im and $AgNO_3$ concentrations from ***AI*** to ***CIV*** changes the preferential growth of surface area from {111} to {110}. Certainly, both C_1-im and $AgNO_3$ play an important role in this process. Recently we reported that the thermolysis of C_1-im and $HAuCl_4$ without $AgNO_3$

Scheme 2. Morphology Change of O_h Symmetric Gold Crystals with Incremental Addition of $AgNO_3$ to a Mixture of [C_1-im]/[Au] at 4/1 Molar Ratio

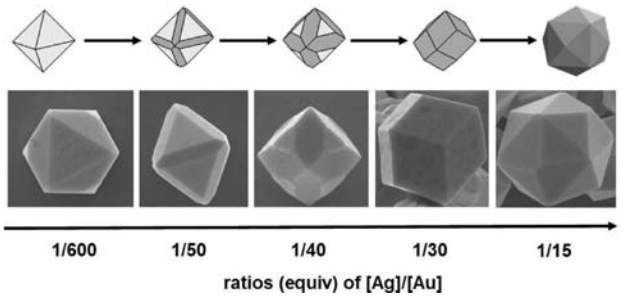

produced highly faceted polyhedrons with mostly {111} facets.[25] It has been suggested that C_1-im, like C_{18}-im, also preferentially adsorbed on Au{111} facets. However, lacking the hydrophobic chain−chain interaction, it functioned only as a capping agent. Without the lamellar templating ability, C_1-im regulated the formation of polyhedrons with mostly {111} facets, in constrast to that of the C_{18}-im, which controlled the formation of Au platelets with extended {111} facets. As known,[7c,d] preferential UPD of Ag on Au{110} facets employing templating agent CTAB has been proposed to account for the observed single crystalline nanorod formation with high energy {110} side facets. In the present work, the effects of combining C_1-im and $AgNO_3$ in the thermolysis with $HAuCl_4$ could be similarly rationalized. We suggest that the capping agent C_1-im also favors the protection of {111} surfaces in the presence of Ag^+, as supported by the observation of strong (111) reflections in Figure 5 ***AI-AIV*** and ***BI***. As for the role of Ag^+, the dual factors of favorable interaction with Au facets and selective UPD on Au facets in the order {110} > {100} > {111} operate in the presence of sterically less demanding C_1-im. The added Ag^+ would persistently adsorb and then reduce on the {110} facets, resulting in a favorable growth of the {110} surface area at increasing $AgNO_3$ concentration. This is supported by the progressive increase of the (220) reflection intensity from ***I*** to ***IV*** in all the ***A***, ***B***, and ***C*** series. Therefore, the competition between the growth of {111} and {110} surfaces is regulated by the relative concentrations of C_1-im and $AgNO_3$, which in turn control the morphology between octahedron and rhombic dodecahedron. Although the details are still not clear, stabilization of high-index Au {210} facets at high C_1-im and $AgNO_3$ concentrations may also account for the formation of Au THH.

Conclusions

A one pot method to fabricate gold crystals through thermolysis of mixtures of *N*-alkylimidazole, $HAuCl_4$, and $AgNO_3$ is described. This simple method does not require additional solvent, template, or protecting agent. The alkyl chain length of the imidazoles and the molar ratios of the [C_n-im]/[Au]/[Ag] mixtures are found to be crucial for the formation of Au crystals. While both the binding energy of Ag^+ with Au facets and the Ag UPD on Au facets follow the order {110} > {100} > {111}, the steric effect of the long alkyl chain in C_{18}-im selectively promotes the Ag deposition on Au{100} rather than the expected {110} facets. Hence in the [C_{18}-im]/[Au]/[Ag] system, preferential stabilization of Au {111} facets by C_{18}-im and protection of Au {100} facets

by Ag lead to the morphology transformation via truncation of an octahedron (with 8 {111} facets) at the vertices covered with {100} facets. For the system of [C_1-im]/[Au]/[Ag], the preferential capping of C_1-im on Au {111} facets and deposition of Ag on Au {110} facets result in the morphology transformation via truncation of an octahedron at the edges covered with {110} facets. This work provides a rare opportunity to observe the dramatic influence of steric effect possessed by the capping agent in the control of Au NCs. The formation of Au THH in high concentrations of C_1-im and $AgNO_3$ is interesting, though its mechanism is not clear. For the first time, the combination of C_n-im and $AgNO_3$ is found to be able to tune a wide range of Au crystal morphologies. This strategy may be applied to the growth of metal crystals in general.

Acknowledgment. We thank the National Science Council of Taiwan for financial support (Grant NSC 97-2113-M-259-012) and National Center for High-Performance Computing (NCHC) of Taiwan for computer resources.

Supporting Information Available: The binding emergies of Ag^+Au_5, Ag^+Au_4, and Ag^+Au_3 are estimated by the B3LYP/LanL2DZ calculations (Table S1). MALDI-TOF spectrum for the organic products after thermolysis. (Figure S1). This material is available free of charge via the Internet at http://pubs.acs.org.